High Spatial Resolution and Sensitivity Laser Cavity Extinction Measurements of Soot Volume Fraction in Nitrogen Diluted Methane Flames

B. Tian*, Y. Gao, S. Hochgreb

Department of Engineering, University of Cambridge, Trumpington Street CB2 1PZ, UK

Abstract

A highly sensitive extinction-based laser cavity soot measurement system with increased spatial resolution is demonstrated, using two partially reflective concave mirrors on either side of the flame under investigation. This configuration makes the beam convergent inside the cavity, allowing for a spatial resolution within 200 μm, whilst increasing the absorption by two orders of magnitude via a multi-pass technique. A series of nitrogen diluted laminar diffusion methane-air flames are tested. Measurements of the soot distribution across the flame show good agreement with results acquired using laser-induced incandescence (LII). The effect of fuel dilution is measured, and the mechanism for the reduction of the net soot production is discussed.

Introduction

Soot particles generated in combustion are both a significant atmospheric pollutant, as well as contributors to climate change [1,2]. As part of research into the development of clean, soot-free combustion systems, inert-diluted hydrocarbon flames are studied since soot production in these flames is significantly lower than in undiluted flames [3–7]. However, accurate, non-invasive techniques for *in situ* measurements of the soot concentration in diluted flames are limited due to the low soot volume fraction (SVF). One of the traditional techniques for SVF measurements is the line-of-sight extinction (LOSE) method [8,9], which it is widely used in calibrating laser induced incandescence (LII) signals [10–13]. LOSE measurements have a number of intrinsic advantages. They provide quantitative measurements of the soot volume fraction and are relatively simple and inexpensive to achieve, given that they only require continuous wave (CW) lasers with relatively low power outputs (tens of milliwatts), and simple photodiodes. However, the extinction-based technique suffers from distinct disadvantages. First, as line-of-sight measurements, they provide an integrated measurement of the soot attenuation along the probe volume, which can only be deconvoluted using a 1D or 2D tomographic algorithm. The signal to noise ratio (SNR) is greatly limited due to low extinction in single-pass configurations. Thus, LOSE measurements cannot be directly applied to flames under diluted conditions. Multi-pass absorption (MPA) techniques, can improve the sensitivity of the technique but may suffer from poor spatial resolution [14,15]. A laser cavity with a pair of mirrors, as employed in the cavity ring-down spectroscopy (CRDS) [12,16,17] and tunable diode laser absorption spectroscopy (TDLAS) methods [18–20] allows for a significant increase in the achievable SNR, while maintaining good spatial resolution.

In the present work, the advantages of LOSE, MPA and the laser cavity technique are combined to develop a high-spatial resolution CW laser cavity extinction technique to measure the SVF from low-soot producing diluted flames. A laser beam cavity is realised by placing two partially reflective concave mirrors on both sides of the target flame. The concave surfaces of the mirrors create a convergent beam inside the cavity, retaining a small beam diameter, which allows for a spatial resolution within 200 μm, whilst increasing the level of absorption by two orders of magnitude. A series of nitrogen diluted laminar diffusion methane flames produced by a Santoro burner are investigated. The measurements of the soot distribution across the flame show good agreement with results using laser-induced Incandescence (LII) from 0.5 ppm to tens of ppb level SVF. A sensitivity analysis is performed in order to ascertain the uncertainty associated with the system, and the influence of inert-dilution in flames on the level of soot formation is also briefly discussed.

CW laser cavity extinction

The LOSE method is based on the fact that light passing through a flame is scattered and absorbed by particles, which results in an attenuation of the beam intensity. This phenomenon is called laser extinction. The extinction ratio (i.e. the intensity ratio of the laser beam before and after the flame, I_t/I_i) for each interval at which the beam passes through the sample is denoted as A. According to the Lambert-Beer Law:

$$\ln \frac{I_t}{I_i} = -\int_{-\infty}^{+\infty} K_e(x)\,\mathrm{d}x = -P_0 \qquad (1)$$

where K_e is the local extinction coefficient of the medium, determined by the local soot volume fraction and its optical properties, and P_0 represents the logarithmic loss of intensity across one pass. The total logarithmic loss of intensity for a cavity, P_t, can be is related to the single pass extinction $A = I_t/I_i = \exp(-P_0)$ via:

$$P_t = \frac{TA}{1-A^2R} \qquad (2)$$

where R and T are the products of the reflectance and transmittance of the two cavity mirrors;. P_t is measured experimentally, and hence the value P_0 can be obtained from Eq. 1 and 2:

$$P_0 = -P_t - \ln\left(\frac{T}{2R}\right) - \ln\left[\sqrt{1+\frac{4R\exp(-P_t)}{T^2}}-1\right] \qquad (3)$$

*Corresponding author: bt312@cam.ac.uk

The value for K_e is computed using a de-convolution algorithm based on Eq. 1 with a three-point Abel transform [21]. The local extinction coefficient, K_e, is determined via the local soot volume fraction. According to Mie scatter theory, the present test is within the Rayleigh approximation. Therefore, by ignoring the contribution of scattering [22,23], the local SVF, f_v , can be obtained from:

$$f_v = \frac{\lambda}{6\pi E(m)} K_e \tag{4}$$

where λ is the wavelength of laser; $E(m)$ is the soot absorption function and is calculated from the soot refractive index m as:

$$E(m)=\mathrm{Im}\left(\frac{m^2-1}{m^2+2}\right) \tag{5}$$

In this study, we assume the value of m to be 1.57-0.56i [24], which is considered a mean value of m in the visible range [25].

Cavity extinction measurement

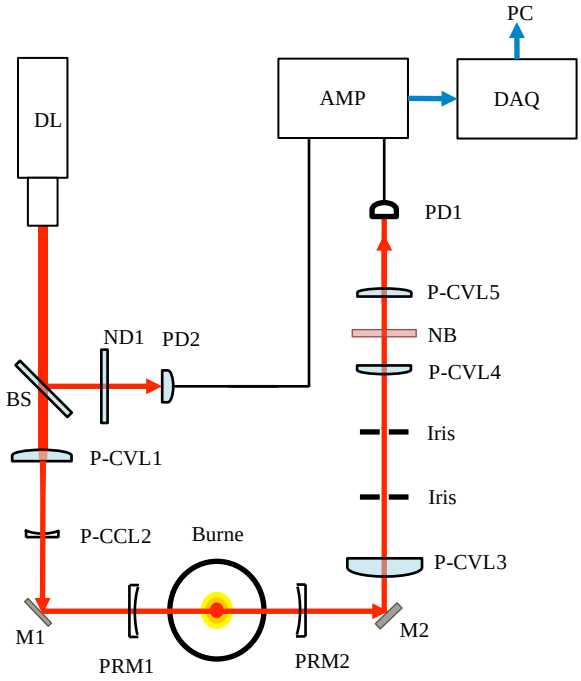

Figure 1. Diagram of the LOSE system (DL: Diode laser; M: mirror; BS: beam sampler; ND: neutral density filter; PD: photodiode; CVL: convex lens; CCL: concave lens; NB: narrow band filter; PRM: partially reflective mirror; AMP: Amplifier; DAQ: data acquisition board

The schematic of the laser cavity measurement system is shown in Fig. 1. A diode laser (Omicron LuxX-638-150, 638 nm wavelength, 150 mW maximum power) is used as the laser source. Near-infrared light is preferred because visible wavelengths can be absorbed by polycyclic aromatic hydrocarbons (PAHs), which contributes to measurement uncertainty. A longer wavelength also means that the Rayleigh approximation for larger soot particles is still valid. The incident beam is split using a beam sampler (Thorlabs BSF05-A) into a reference beam ⩽1% of the power), and the probe beam. A neutral density filter ND1 (Thorlabs NE40A, optical density=4.0) is used to attenuate the beam density to a range suitable for the reference photodiode. The probe beam is focused using a plane-convex lens (P-CVL1, Thorlabs LA1301-A, 250 mm focal length) and a plane-concave lens P-CCL (Thorlabs LC4888, -100 mm focal length) down from a 1.1 mm (diameter) beam of ⩽0.5 mm diameter before entering the cavity. The two cavity mirrors PRM1 (COMAR Optics customised, 1000 mm focal length, reflectivity: 98.11%±0.20%, transmittivity: 1.530%±0.147% at 638 nm wavelength), PRM2 (COMAR Optics customised, 1000 mm focal length, reflectivity: 98.11%±0.19%, transmittivity: 1.537%±0.159% at 638 nm wavelength) are aligned at opposite ends, with the burner in the middle. The detection system consists of two identical photodiodes, PD1 and PD2 (Thorlabs SM05PD1A Silicon Photodiode, 350-1100 nm, cathode grounded), which detect the light sampled from the transmitted and reference beam, respectively. The photocurrents obtained from the two photodiodes PD1 and PD2 are assumed to be linearly proportional to the respective incident intensities, and compared by a logarithmic amplifier (Texas Instrument LOG104), which improves the SNR relative to a linear amplifier for this application. The output voltage of the amplifier, V, is measured allowing P_t to be evaluated.

The experiments were performed on a standard Santoro laminar diffusion burner [22]. The diameter of the inner fuel tube is 10.5 mm, and that for the outer air co-flow tube is 96.8 mm. The burner is mounted on a traverse platform to scan through the flame at various positions with a precision of 0.01 mm along the horizontal direction and 0.5 mm along the vertical. The test conditions are grouped into five categories (from group A to E). In each group, the methane flow rate is kept constant while varying nitrogen flow rate. The total carbon flow rate remains the same, while the mole fraction of fuel in the fuel flow ($X_{\mathrm{f,in}}$) changes. The operating conditions are listed in Table 1. Figure 2 shows natural light photos of the 16 flames under consideration. Each flame is labeled with a letter and a one or two digit number. For example, flame A05 represents the flame in group A with a nitrogen flow rate of 0.05 slpm and flame E2 represents a group E flame with a nitrogen flow rate of 0.1 slpm. Flame D0 and E0 (non-diluted conditions) have been tested by Shaddix *et al.* [10,26] in previous work. Based on flame D0 and E0, the fuel flow rate is decreased from group E to that of group A, while nitrogen dilution is gradually increased in each flame.

Case	A		B		C			D			
	A0	A05	B0	B1	C0	C1	C2	D0	D1	D2	D3
CH_4 mass flow rate (slpm)	0.19		0.24		0.30			0.40			
Air mass flow rate (slpm)	16.2		20.5		25.6			35.0			
N_2 mass flow rate (slpm)	0	0.05	0	0.10	0	0.10	0.20	0	0.10	0.20	0.30
$X_{f,\,in}$ in fuel flow (%)	100	79.2	100	70.6	100	75.0	60.0	100	80.0	66.7	57.1

Case	E				
	E0	E1	E2	E3	E4
CH_4 mass flow rate (slpm)			0.53		
Air mass flow rate (slpm)			65.8		
N_2 mass flow rate (slpm)	0	0.10	0.20	0.30	0.40
$X_{f,\,in}$ in fuel flow (%)	100	84.1	72.6	63.9	57.0

Table 1: Test conditions for normal and nitrogen diluted laminar CH_4-air diffusion flames

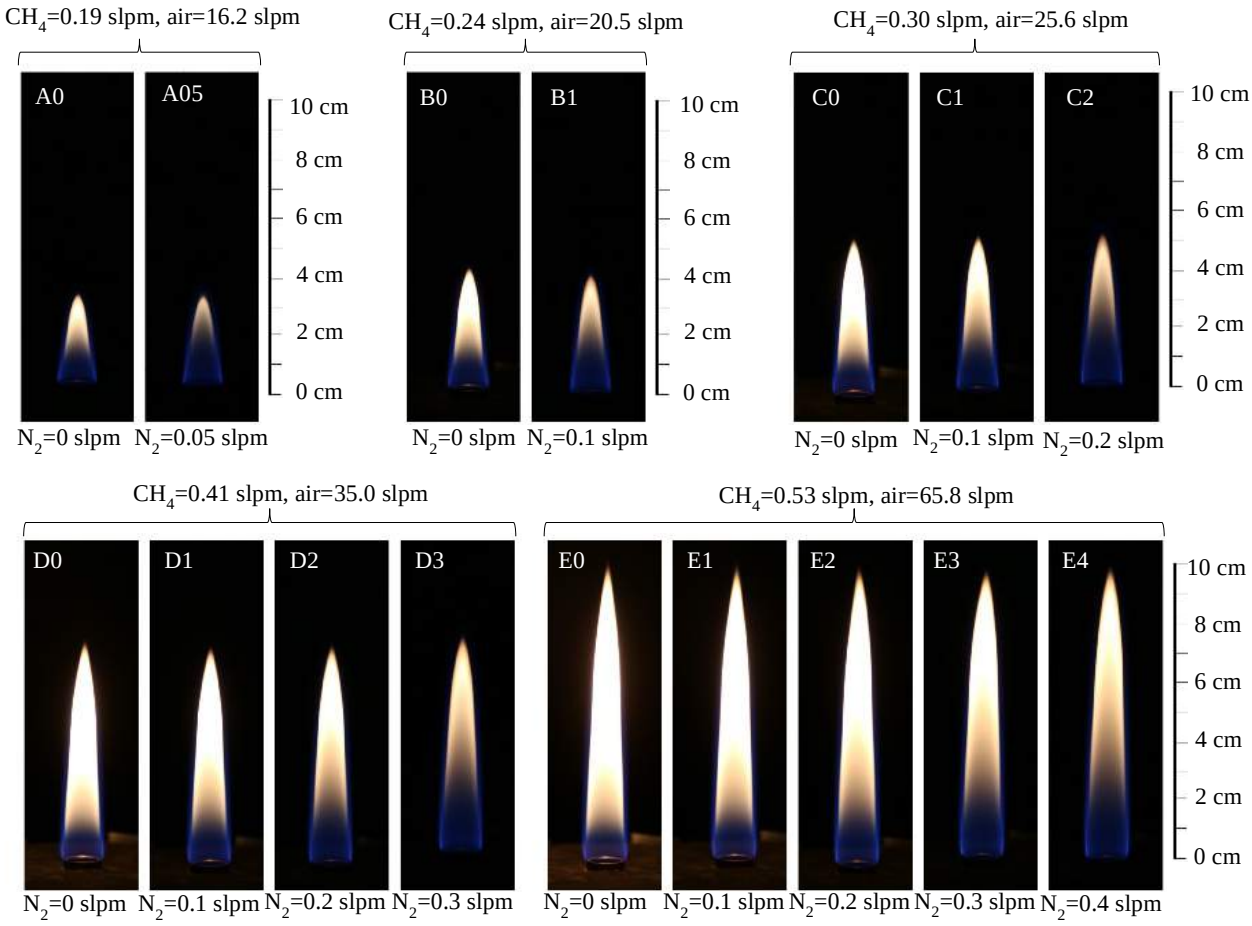

Figure 2: Natural luminosity of laminar diffusion flames tested (Camera model: Canon EOS 6D DLSR, exposure time=1/60 s, Photographic Sensitivity (ISO) =1250; Lens Model: Canon EF 24-105mm f/4L IS, f=4.0, focal length=105 mm)

Laser induced incandescence measurement

The 2D LII measurements were performed using the setup illustrated in Fig. 3. The laser source is a 532 nm Nd:YAG laser (Litron nanoPIV) firing at 10-25 Hz. The beam was collimated into a parallel sheet using a series of beam shaping optics (Thorlabs cylindrical lens with focus lengths of 75 mm, -25 mm and 100 mm respectively). It is then passed through an aperture to generate a top-hat profile. The beam energy profile was detected by passing it through a cuvette filled with fluorescent dye (Rhodamine 6G in ethanol solvent) and imaging the fluorescence using a CCD camera (LaVision Imager Pro X 4M, 1 μs gate width, 1024×1024 pixels) equipped with a Nikon AF Micro Nikkor 60 mm lens (f/5.6) and a narrow band filter (Thorlabs FB600-10, central wavelength=600±2 nm, FWHM=10±2 nm). The LII signal induced by the laser sheet was captured using an ICCD camera (LaVision

Intensified Relay Optics and Imager Pro X 4M, 1024×1024 pixels) through a Nikon AF Micro Nikkor 60 mm lens 175 (f/2.8) and a band-pass filter (Thorlabs FB400-40, central wavelength=400±8 nm, FWHM=40±8 nm) to minimize luminosity from PAH fluorescence, C_2 radiation and flame. A gate width of 100 ns was selected to maximize the signal-to-noise ratio. The spatial resolution of each image is 33 μm/pixel.

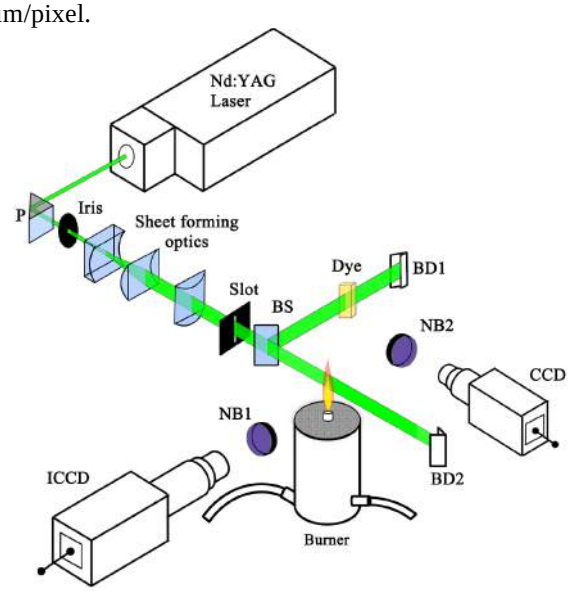

Figure 3: Schematic of LII measurement setup (P: prism; BS: beam splitter; NB1: 400±20 nm band filter; NB2: 600±5 nm band filter; BD: beam dump).

The LII signal response to the laser fluence was tested and optimised. The LII images are calibrated using the extinction data by considering that the integrated total soot volume fraction across the centreline chord at a particular height yields a total projected signal P_0. We assume that the LII signal is proportional to the soot volume fraction [27,28], with a linear coefficient K_{LII}:

$$P_{0,\text{centre}} = K_{LII}\frac{6\pi E(m)}{\lambda}\int_{-\infty}^{+\infty} S_{LII}(r)\,dr \qquad (6)$$

where S_{LII} is LII signal intensity as a function of radial distance r. Eq. 6 can be solved for K_{LII} if the projected loss is known at a particular height.

Figure 4. LII images for flame A0 to E4

Results and discussion

Figure 4 shows the captured LII images for each test case. In order to accommodate for the length-to-width ratio of the flames, three different series of images were taken, with images connecting at heights of 34 and 68 mm. Figure 4 shows that there is a dramatic decrease in SVF with a decrease in the CH_4 mole fraction $X_{f,\,in}$ in the fuel line. A plot of the peak SVF against the N_2 mole fraction $X_{N_2,\,in}$ in fuel flow is given in Fig 5.

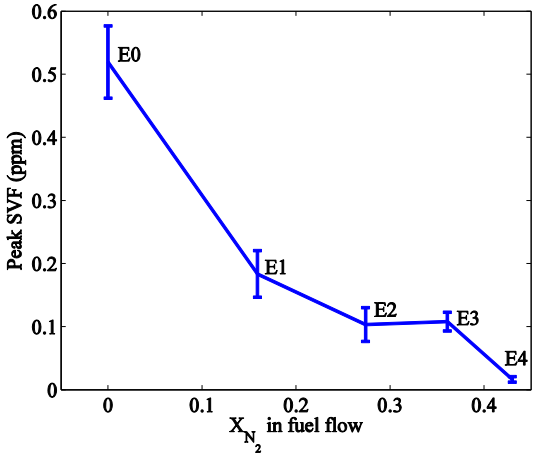

Figure 5: Peak SVF vs N_2 mole fraction $X_{N_2,\,in}$ of group E flame

From flames E0 to E4, where dilution gas mole fraction $X_{N_2,in}$ increases by a factor of 1.75, the peak SVF decreases by a factor of 50. This is a consequence of the fact that the nitrogen diluent not only changes the flame temperature, but also reduces $X_{f,\,in}$ in the fuel flow [4]. To isolate the two effects, we assume initially that the flame temperature is equal to adiabatic equilibrium temperature: $T=T_{ad}$, as calculated using Cantera with GRI3.0 thermodynamics [29]. The result is plotted using a blue line in Fig. 6. The results indicate that for values of $X_{N_2,in}$ ranging from 0 to 0.6, the dependence of temperature on $X_{N_2,in}$ is not strong. If we assume that the mole fraction of oxygen in the oxidizer flow is constant, a one-step global reaction rate can be approximated proportional to an Arrhenius term:

$$w \sim A_G (1 - X_{N_2,in})^{\alpha} \exp\left(\frac{-E_a}{R_0 T_{ad}(X_{N_2,in})}\right) \qquad (7)$$

For α=1, the effect of $X_{N_2,\,in}$ can be isolated as shown in Fig. 6 by keeping the reaction temperature to the undiluted adiabatic temperature $T_{ad}(X_{N_2,\,in}=0)$ (green line), which has a linear relationship to $X_{N_2,\,in}$. The overall reaction rate changes exponentially with the local temperature, as indicated by the red line, for a global activation energy $E_a=2.9\times10^5$ J/mol, suggested by Venkatesh *et al* [30]. Figure 6 indicates that, for α=1, the effect of temperature change is not as significant as the change in reactant concentration.

Both extinction and LII measurements are applied to flames A0 to E4. Figure 7 shows the comparison between the results obtained using the two measurement techniques on flame D2. Error bars for the LII measurements are obtained from the standard deviation of LII signals over 500 images, and the error bars of extinction are directly calculated from the standard deviation of raw data by error propagation. The two measurements yield good agreement after a single calibration for each fuel, even in the sub-ppm range. The uncertainty associated with the extinction measurements gradually increases towards the flame centre. This is due to the cumulative effects of Abel transform [21]. The result shows that, for the measurement of a stable annular soot distribution field using flames similar to the present study, the measurement uncertainty of this cavity system can be as low as 20 ppb in the edge region and 0.1 ppm in centre region. If the system is applied to a homogenous measurement volume or sampling cells, the accuracy can be increased even further.

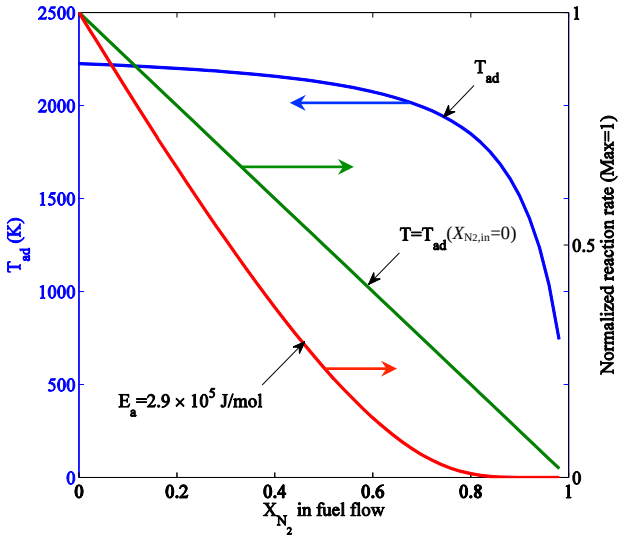

Figure 6: Adiabatic temperature as a function of N_2 mole fraction $X_{N_2,\,in}$ (left); normalised global reaction rate for a given activation energy E_a [30]

Conclusion

A laser-cavity extinction technique with high-spatial resolution is developed to measure the soot volume fraction across nitrogen diluted, low soot producing laminar methane-air diffusion flames. Inert dilution decreases the yield of soot by several orders of magnitude. Comparisons with LII measurements on low sooting flames show good agreement with cavity extinction measurements. Data analysis shows that for a stable measurement target, without flickering, a measurement error of less than 20 ppb can be achieved, resulting in a measurement range in tens of ppbs. High spatial resolution of 200 μm can be achieved by using concave cavity mirrors in the optical set-up.

Acknowledgements

The authors thank the financial support from China Scholarship Council. We sincerely thank Dr W. Cai for his help in the development of laser-cavity system. We also thank Dr S. Balusamy and Mr S. Lowe for their help during the experiments.

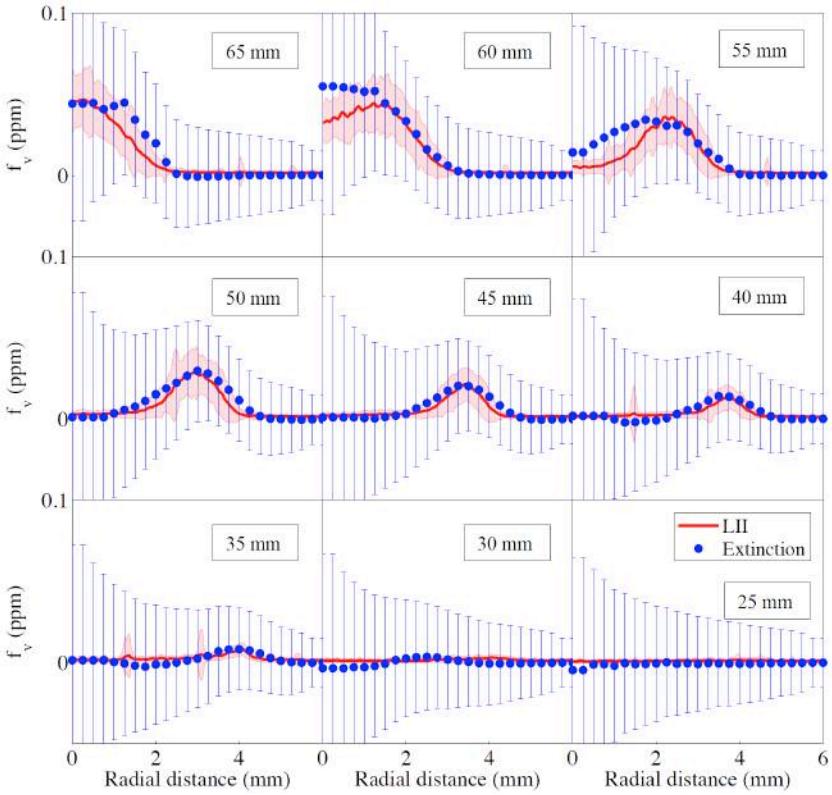

Figure 7: Soot volume fraction f_v using cavity extinction (blue circles with blue error bar) and and LII (red line with translucent error shadow) for flame D2 at different heights above burner (HAB)

References

[1] Service RF. *Science* (80) 2008;319:1745.
[2] Wang H. *Proc. Combust. Inst.* 2011;33:41–67.
[3] Du D, Axelbaum R, Law C. *Combust. Flame* 1995;2180:11–20.
[4] Axelbalim R, Flower W, Law C. *Combust. Sci. Technol.* 1988;61:51–73.
[5] Flügel A, Kiefer J, Leipertz A. *Proc. Eur. Combust. Meeting* 2009.
[6] Min J, Baillot F, Guo H, Domingues E, Talbaut M, Patte-Rouland B. *Proc. Combust. Inst.* 2011;33:1071–8.
[7] Oh K, Shin H. J. *Mech. Sci. Technol*. 2005.
[8] Snelling DR, Smallwood GJ, Liu F, Gülder ÖL, Bachalo WD. *Appl. Opt*. 2005;44:6773.
[9] Di Sante R. Opt. Lasers Eng. 2013;51:783–9.
[10] Shaddix C, Smyth K. *Combust. Flame* 1996;107:418–52.
[11] Schulz C, Kock BF, Hofmann M, Michelsen H, Will S, Bougie B, et al. *Appl. Phys. B* 2006;83:333–54.
[12] Desgroux P, Mercier X, Lefort B, Lemaire R, Therssen E, Pauwels JF. *Combust. Flame* 2008;155:289–301.
[13] Karataş AE, Gülder ÖL. Prog. *Energy. Combust. Sci* 2012;38:818–45.
[14] Manninen A, Tuzson B, Looser H, Bonetti Y, Emmenegger L. *Appl. Phys. B* 2012;109:461–6.
[15] Krzempek K, Jahjah M, Lewicki R, Stefański P, So S, Thomazy D, et al. *Appl. Phys. B* 2013;112:461–5.
[16] Bouvier Y, Mihesan C, Ziskind M, Therssen E, Focsa C, Pauwels JF, et al. *Proc. Combust. Inst.* 2007;31:841–9.
[17] Vander Wal RL. *Proc. Combust. Inst.* 1998;27:59–67.
[18] Cai W. Appl. Phys. Lett. 2014;104:154106.
[19] Wagner S, Fisher BT, Fleming JW, Ebert V. *Proc. Combust. Inst.* 2009;32:839–46.
[20] Basu S, Lambe DE, Kumar R. *Int. J. Heat Mass Transf.* 2010;53:703–14.
[21] Dasch CJ. *Appl. Opt.* 1992;31:1146–52.
[22] Santoro RJ, Semerjian HG, Dobbins R. *Combust. Flame.* 1983;51:203–18.
[23] Liu F, Thomson K, Smallwood GJ. *Appl. Phys. B* 2009;96:671–82.
[24] D'Alessio A, Di Lorenzo A, Beretta F, Venitozzi C. *Proc. Combust. Inst.* 1973;14:941–53.
[25] Smyth K, Shaddix C. *Combust. Flame* 1996;107:314–20.
[26] Shaddix CR, Harrington JE, Smyth KC. *Combust. Flame* 1994;99:723–32.
[27] Liu F, Smallwood GJ. *Appl. Phys. B* 2013;112:307–19.
[28] Bladh H, Johnsson J, Bengtsson P-E. *Appl. Phys. B* 2007;90:109–25.
[29] Smith G, Golden D, Frenklach M, Moriarty N, Eiteneer B GM. *http://www.me.berkeley.edu/gri_mech/.*
[30] Venkatesh S, Saito K. *Combust. Sci. Technol.* 1992;85:297–311.